PHYSICAL REVIEW B VOLUME 35, NUMBER 4 1 FEBRUARY 1987

# Light scattering from magnons in $MnF_2$

D. J. Lockwood and M. G. Cottam*
*Physics Division, National Research Council, Ottawa, Canada K1A 0R6*
(Received 22 August 1986)

We report measurements for the temperature dependence and polarization dependence of the one-magnon and two-magnon Raman scattering in the rutile-structure antiferromagnet $MnF_2$. The frequencies and integrated intensities of the excitations over the temperature range 4—50 K are found to be in good agreement with the theoretical analysis. For one-magnon scattering we deduce that the linear magneto-optic coupling is dominant. This contrasts with the situation in isostructural $FeF_2$ where quadratic coupling is known to be important. From the two-magnon results numerical values are obtained for the relative magnitudes of the magneto-optic coupling coefficients, and in this case the results are found to be broadly similar to $FeF_2$.

## I. INTRODUCTION

In this paper we present new experimental and theoretical results concerning light scattering from magnons in the antiferromagnet $MnF_2$ ($T_N = 68$ K, $S = \frac{5}{2}$). This material has the rutile crystal structure (space group $P4_2/mnm$, or $D_{4h}^{14}$) and, along with the isomorphous $FeF_2$, it has been extensively studied because of the relative simplicity of the magnetic ordering.

The two-magnon scattering in $MnF_2$ is relatively strong, and its magnetic Raman spectrum was one of the first to be investigated experimentally.[1,2] These and subsequent[3–7] measurements established that the two-magnon Raman spectrum exhibits a strong dependence on the polarizations of the incident and scattered light. Theories for two-magnon light scattering have been developed by several authors, covering temperature ranges below and above $T_N$, and we refer to Refs. 8 and 9 for review accounts. We have extended the previous work by making detailed experimental measurements of the polarization dependence of the two-magnon spectrum, and the comparison with theory allows the relative values of the magneto-optic coupling coefficients to be deduced for the first time. The behavior is compared with that of $FeF_2$ where a similar analysis of the two-magnon Raman scattering was recently reported.[10]

By contrast, the one-magnon scattering in pure $MnF_2$ is extremely weak, and the present work represents its first experimental observation. Preliminary accounts have appeared elsewhere,[11,12] and we now give a more extended description and analysis of the results. In fact there have been no reported measurements of one-magnon light scattering in other pure manganese compounds.[9,13] In the first theory[2] of such scattering it was proposed that the intensity is expected to be weak because it is proportional to the square root of the effective anisotropy field, $H_A$, which is generally small in $S = \frac{5}{2}$ insulators.[9,13] However, one-magnon Raman scattering has been observed from the manganeselike mode in the mixed antiferromagnets $Co_xMn_{1-x}F_2$, $Fe_xMn_{1-x}F_2$, and $Cd_xMn_{1-x}Te$.[14–16] The scattering associated with the $Mn^{2+}$ ions in these mixed compounds is found to be relatively strong at intermediate concentrations, $x$, but becomes weak and eventually unobservable as $x$ tends to zero.[14,15] From the $Co_xMn_{1-x}F_2$ work it was inferred that the absence of an orbital angular momentum contribution to the magnon state may also lead to a small one-magnon scattering cross section.[14] The experiments described in this paper for one-magnon Raman scattering in pure $MnF_2$ enable a detailed analysis to be made of the magnon temperature dependence (up to about 50 K) and of the nature of the magneto-optic coupling. The results in the latter case are shown to be quite different from those for another rutile-structure antiferromagnet, $FeF_2$.[17]

In the next section we describe the experiments and we present results for the one-magnon and two-magnon Raman scattering in $MnF_2$. The theoretical analysis of the one-magnon frequency and damping, and their temperature dependences, is given in Sec. III, while the weak one-magnon intensities are analyzed in Sec. IV. The polarization dependence and temperature dependence of the more intense two-magnon scattering are discussed in Sec. V, where we deduce the relative values of the magneto-optic coupling coefficients. The conclusions are given in Sec. VI, where we compare and contrast light scattering from magnons in $MnF_2$ and $FeF_2$.

## II. EXPERIMENT

The pale-orange color $MnF_2$ crystal used in these experiments was grown especially for this work at the Clarendon Laboratory of Oxford University. The crystal boule was x-ray oriented and cut to provide a cuboid sample of dimensions 5.5, 5.8, and 6.0 mm along the crystallographic $a$, $b$, and $c$ axis directions, respectively. The sample faces were polished with 1-$\mu$m diamond powder. The resulting specimen was generally of high optical quality: It did possess a few bubblelike major internal defects, but these were easily avoided in the experiment.

Measurements of the optical-absorption spectrum of $MnF_2$ showed that, for the available argon laser wavelengths in the visible, the lines at 457.9 and 476.5 nm were in a region of low absorption. However, because of the high laser power needed to see the weak magnetic excitations, only the line at 476.5 nm was used in this study. Excitation at 476.5 nm had the added advantage of placing the Raman shifted lines at wavelengths below the

strong pink luminescence exhibited by $MnF_2$.

The two-magnon Raman spectrum was excited with approximately 600 mW of filtered argon laser light at 476.5 nm, while approximately 760 mW was used for the one-magnon measurements. The light scattered at 90° was analyzed using a Polaroid polarizer, dispersed with a Spex 14018 double monochromator (with blazed holographic gratings) at a spectral resolution of $1.8\pm0.1$ cm$^{-1}$, detected with a cooled RCA 31034A photomultiplier, and recorded under computer control.[9] A diamond-shaped mask provided by Spex was placed over the first grating of the double monochromator for all measurements and was essential for observing the one-magnon line, as it reduces the stray exciting-light intensity on the Stokes-shift side of the laser line. The sample was mounted in the helium exchange-gas space of a Thor S500 cryostat, where the temperature was controlled to within 0.1 K. Despite the high incident powers, the local laser heating estimated from the phonon anti-Stokes—Stokes scattering was found to be small [$\sim0.5$ ($\sim0.7$) K at $\sim600$ ($\sim760$) mW laser power] as a result of the low crystal absorption. The sample temperature, as measured with a gold-iron—Chromel thermocouple, has been corrected for this local heating effect. The $X$, $Y$, and $Z$ laboratory axes used to describe the scattering configuration and scattered light polarization lie along the crystal $a$, $b$, and $c$ axes, respectively.

The low-frequency Raman spectrum of $MnF_2$ recorded as a function of temperature for $T < T_N$ is shown in Fig. 1. A Raman line was found at 8.5 cm$^{-1}$ for $T \ll T_N$ that shifted to lower frequency with increasing temperature. The line was observed in $Z(XZ)Y$ and $Z(YZ)Y$ polarizations (see Fig. 1) but was not detected in $Z(YX)Y$ or $Z(XX)Y$ polarizations. It was also observed weakly in $X(ZX)Y$ polarization at 7 K, but in this scattering geometry the stray light was higher and it precluded a detailed study of the temperature dependence. A search for this line in anti-Stokes scattering proved unsuccessful, because of a higher instrumental stray-light background on the low-wavelength side of the exciting line.

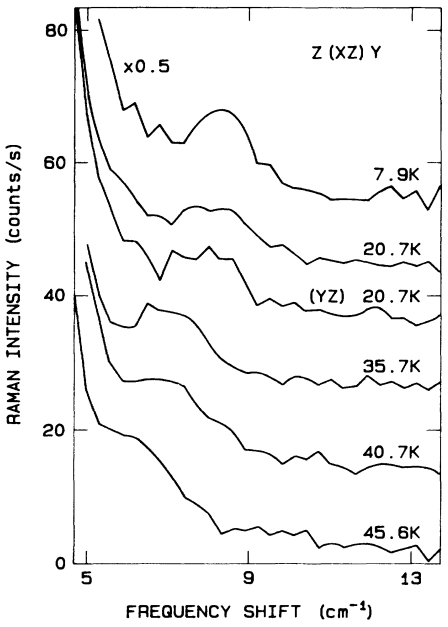


FIG. 1. Temperature dependence of the low-frequency Stokes-Raman spectrum of $MnF_2$ recorded in $Z(XZ)Y$ polarization and in $Z(YZ)Y$ polarization [denoted by $(YZ)$ in the figure].

The polarization characteristics and temperature dependence of the 8.5-cm$^{-1}$ line indicate that it can be assigned to one-magnon scattering. The magnon frequency at $T \ll T_N$ is in good agreement with the antiferromagnetic resonance value of 8.7 cm$^{-1}$.[18] The spectra were least-squares fitted to a model comprising a damped harmonic-oscillator function of the form

$$I(\omega)=[n(\omega)+1]P\omega_M^2\Gamma^2\omega/[(\omega^2-\omega_M^2)^2+\Gamma^2\omega^2] \quad (1)$$

together with a Gaussian function, which was proved from the $Z(YX)Y$ spectrum to represent accurately the instrumental (background) line shape. In Eq. (1), $P$, $\omega_M$, and $\Gamma$ are the oscillator strength, frequency, and damping, respectively, and $n(\omega)$ is the Bose population factor evaluated at frequency $\omega$. The parameter values obtained from the fits are presented in Sec. III.

The two-magnon scattering in $MnF_2$ is known from earlier work to occur at frequencies below 120 cm$^{-1}$.[1,2] Some of the results obtained here for the temperature and polarization dependences of the scattering are shown in Figs. 2, 3, and 4. In their general details the results parallel those of earlier workers[1-7] in that a broad (compared with the one-magnon line) asymmetric line is observed at low temperatures that shifts to lower frequency with increasing temperature. The two-magnon scattering is still observable as a wing feature for $T \gtrsim 4T_N$. The polarization measurements at low temperature reveal the clear difference in the two-magnon line shapes for scattering in $(YZ)$ [or $(ZX)$] and $(YX)$ polarizations and, for the first

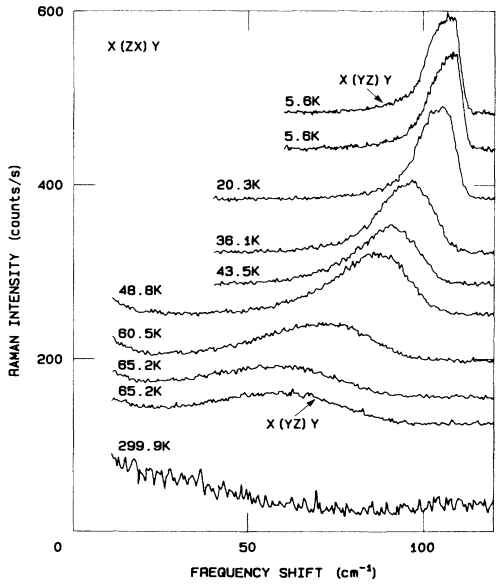


FIG. 2. Temperature dependence of the two-magnon scattering in $MnF_2$ in $(ZX)$ and $(YZ)$ polarizations.

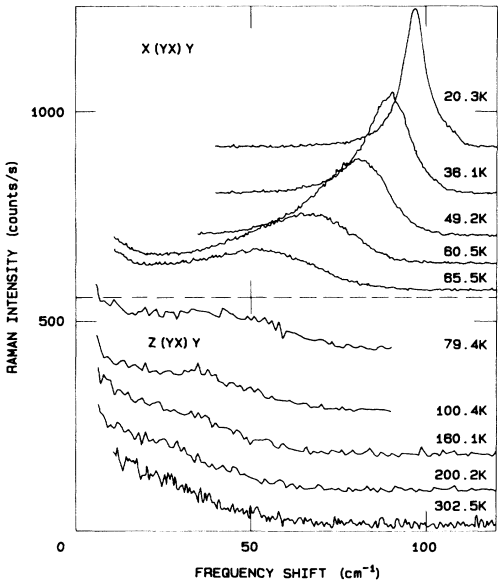


FIG. 3. Temperature dependence of the two-magnon scattering in $MnF_2$ in ( $YX$) polarization.

time, the presence of a weak and very broad two-magnon scattering in ($XX$) and ($ZZ$) polarizations. The band parameters of peak frequency and integrated intensity were extracted by a computer analysis of the data, while the linewidth [full width at half maximum (FWHM)] was determined manually. The results of this analysis are presented in Sec. V.

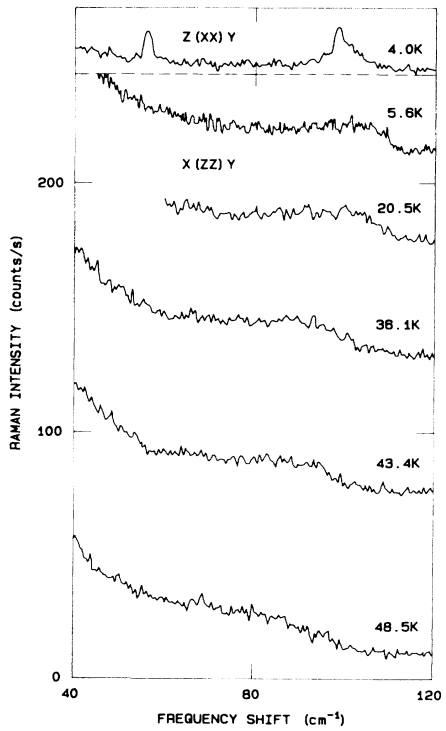


FIG. 4. The two-magnon Raman spectrum of $MnF_2$ in ($XX$) and ( $ZZ$) polarizations.

## III. ANALYSIS OF ONE-MAGNON FREQUENCY AND DAMPING

To analyze the experimental data we represent $MnF_2$ by the spin Hamiltonian

$$H=\sum_{i,j}J_{ij}\mathbf{S}_i\cdot\mathbf{S}_j+\tfrac{1}{2}\sum_{i,i'}J'_{ii'}\mathbf{S}_i\cdot\mathbf{S}_{i'}+\tfrac{1}{2}\sum_{j,j'}J'_{jj'}\mathbf{S}_j\cdot\mathbf{S}_{j'}$$
$$-g\mu_B H_A(T)\left[\sum_i S_i^z-\sum_j S_j^z\right]. \quad (2)$$

Here $i$ and $i'$ denote sites on sublattice 1 (spins predominantly "up") and $j$ and $j'$ denote sites on sublattice 2 (spins predominantly "down"). Equation (2) includes effects of intersublattice exchange $J_{ij}$ and also the weaker intrasublattice exchange $J'_{ii'}$ and $J'_{jj'}$. The quantity $H_A(T)$ is a temperature-dependent effective field representing the uniaxial anisotropy. The approximate values of the parameters in Eq. (2) are known from neutron scattering experiments,[19] which show that three types of exchange constants may need to be considered. These are indicated in Fig. 5 which illustrates the rutile crystal structure of $MnF_2$. The dominant exchange is provided by the interaction $J_2$ between a $Mn^{2+}$ ion and its eight next-nearest neighbors on the opposite sublattice, while $J_1$ and $J_3$ represent intrasublattice exchange coupling to nearest and third-nearest neighbors, respectively.

For discussion of the *one-magnon* data (at $\mathbf{k}\approx\mathbf{0}$) it is, in fact, a good approximation to neglect the effects of $J_1$ and $J_3$ compared with $J_2$, and we employ the values $J_2=2.45$ cm$^{-1}$ and $g\mu_B H_A(0)=0.74$ cm$^{-1}$. The temperature dependence of the anisotropy is conventionally introduced by writing $H_A(T)\propto\langle S^z\rangle^n$, where $\langle S^z\rangle$ is the sublattice spin average and $n$ is a positive index. If $H_A(T)$ were due to single-ion anisotropy (e.g., as in $FeF_2$) the appropriate choice would be $n=2$, but for $MnF_2$ it has been estimated[20,21] that the anisotropy comes predominantly from magnetic dipole-dipole interactions and the value of $n$ may be modified accordingly. If the neighboring spins are considered as being either completely uncorrelated (that is, $\langle S_iS_j\rangle=\langle S_i\rangle\langle S_j\rangle$ for $i\neq j$ as in mean-field theory) or strongly correlated, then this would lead to $n=1$ and $n=2$, respectively, as limiting values.[22] A low-temperature spin-wave theory for dipolar anisotropy has been carried out by Oguchi,[22] and for $MnF_2$ his results would imply $n=1.9$ at $T\lesssim 20$ K. This is broadly

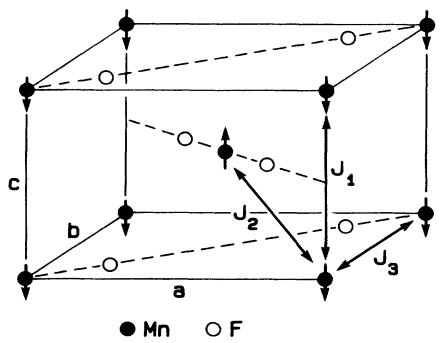


FIG. 5. The crystallographic unit cell of $MnF_2$ with the principal exchange interactions marked.

consistent with antiferromagnetic resonance (AFMR) data[18] for these temperatures. A similar value, namely $n=1.88\pm0.16$, has been deduced experimentally at higher temperatures ($50\ \mathrm{K} < T \lesssim T_N$) using AFMR and sublattice magnetization data.[23] However, it is unclear whether this dependence persists at intermediate temperatures from about 20 to 50 K, or whether a mean-field type of approximation ($n=1$) is appropriate. In view of this uncertainty we consider two cases, $n=1$ and $n=2$, in analyzing our Raman data.

First we discuss the frequencies of the one-magnon excitations. The simplest theory incorporating temperature-dependent effects is linear spin-wave theory with the random-phase approximation (RPA) used to decouple the exchange terms. This leads to an expression for the $\mathbf{k}=\mathbf{0}$ magnon frequency $\omega_M$ of the familiar form[2,21]

$$\omega_M=[\omega_A(2\omega_E+\omega_A)]^{1/2}\ , \tag{3}$$

where $\omega_A=g\mu_B H_A(T)/\hbar$ and $\omega_E=8\langle S^z\rangle J_2/\hbar$ are temperature-dependent anisotropy and exchange frequencies, respectively. The static thermal average $\langle S^z\rangle$ can be evaluated in terms of the Brillouin function for $S=\frac{5}{2}$. Some numerical results are shown in Fig. 6, where the dashed and solid theory curves correspond to $n=1$ and $n=2$, respectively, and comparison is made with the experimental data. Although the overall agreement between theory and experiment is fairly good, particularly for the $n=1$ curve in Fig. 6, we have made further calculations to allow for the effects of magnon-magnon interactions. These may be important and their inclusion should lead to a more accurate theory. We employ the high-density perturbation method of Cottam and Stinchcombe,[24] and when this is modified for $S=\frac{5}{2}$ systems[25] and applied to $MnF_2$ we obtain the theory curves in Fig. 7. In this case it is necessary to perform numerical integrations over wave vectors in the first Brillouin zone, and approximations have been made which limit the validity to $T \lesssim 42$ K. It can be seen from Fig. 7 that when magnon-magnon interactions are taken into account it is the $n=2$ curve that gives better agreement with experiment.

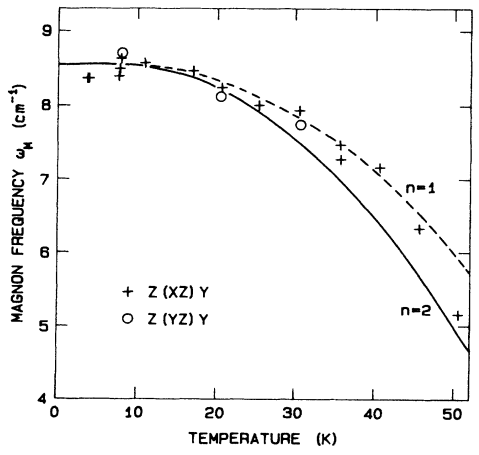


FIG. 6. Comparison of theory and experiment for the temperature dependence of the Stokes one-magnon peak frequency in $MnF_2$. The experimental data are from $Z(XZ)Y$ (crosses) and $Z(YZ)Y$ (circles) polarizations and the curves are from the theory excluding magnon-magnon interactions for the cases of $n=1$ (dashed line) and $n=2$ (solid line).

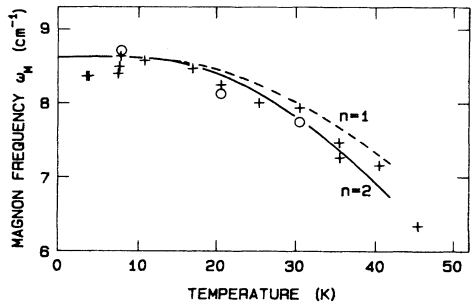


FIG. 7. As for Fig. 6, but with the theory curves calculated from the model including magnon-magnon interactions.

The data for the temperature dependence of the one-magnon linewidth are summarized in Fig. 8. It can be seen that the linewidth (FWHM) increases from about 2.4 cm$^{-1}$ at 4 K to about 3.8 cm$^{-1}$ at 45 K. When allowance is made for the instrumental resolution of 1.8 cm$^{-1}$, the above values correspond to an increase in the damping half-width of the magnons from approximately 0.3 to 1 cm$^{-1}$ over the temperature range. Hence the one-magnon damping at $\mathbf{k}\approx\mathbf{0}$ in $MnF_2$ is much smaller than measured for $FeF_2$.[3,17] On the theoretical side, there are two mechanisms commonly employed for the magnon damping in *Heisenberg* antiferromagnets. One is the usual four-magnon relaxation process,[26] and the other is magnon scattering by the longitudinal spin disorder.[24,25,27] The former process should be dominant at low temperatures $T \ll T_N$, while the latter becomes important nearer $T_N$. In fact, Stinchcombe and Reinecke[25] have shown that the latter mechanism accounts well for the magnon damping in $MnF_2$ at nonzero $\mathbf{k}$ and $T \gtrsim 60$ K as determined from neutron scattering data.[28] However, $\mathbf{k}\approx\mathbf{0}$ and for the range of lower temperatures considered here, we estimate that the above two mechanisms predict a *thermal* damping much smaller than is observed experimentally. Other

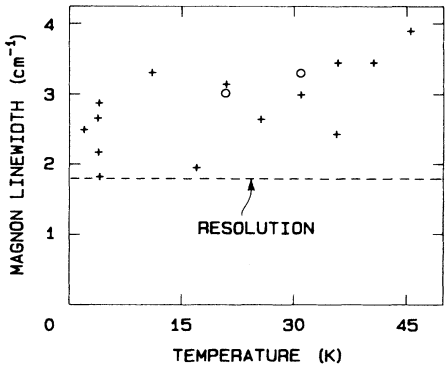


FIG. 8. Temperature dependence of the one-magnon linewidth (FWHM) in $MnF_2$. The polarization notation for the experimental points is the same as in Fig. 6.

contributions to the magnon damping could arise due to interactions with phonons or due to dipole-dipole interactions, but quantitative estimates are not currently available for $MnF_2$ over the full temperature range considered.

## IV. ANALYSIS OF THE ONE-MAGNON INTENSITIES

To discuss the Raman intensity we use a Green-function theory[29] which allows for the inclusion of magneto-optic coupling quadratic in the spin operators, as well as the usual linear magneto-optic coupling.[2] Since the symmetries of the two sublattices in $MnF_2$ are not equivalent, due to the coordination of the $F^-$ ions (see Fig. 5), there may also be an out-of-phase contribution to the scattering as well as the in-phase contribution. This model has successfully accounted for the polarization dependence and temperature dependence of the one-magnon Raman intensity in $FeF_2$.[17] The quadratic magneto-optic coupling has a large effect in $FeF_2$, and it is of interest to study the nature of the magneto-optic coupling in $MnF_2$ which has a similar magnetic ordering.

For Stokes scattering in zero-applied magnetic field, the integrated intensity $I_S$ takes the general form[29]

$$I_S = A\langle S^z\rangle (n_M+1)(F_{\text{in}}+F_{\text{out}})/\omega_M \ . \tag{4}$$

Here the overall factor $A$ is independent of temperature and scattering geometry, and the Bose factor $n_M$ is

$$n_M = [\exp(\hbar\omega_M/k_BT)-1]^{-1} \tag{5}$$

with the magnon frequency $\omega_M$ given in Eq. (3). The quantities $F_{\text{in}}$ and $F_{\text{out}}$, which refer to in-phase and out-of-phase scattering, are

$$F_{\text{in}} = |\, e_A^- \omega_A^{1/2} K_+ - 2p\langle S^z\rangle e_S^- (2\omega_E+\omega_A)^{1/2} G_+ \,|^2 \ , \tag{6}$$

$$F_{\text{out}} = |\, e_A^+ (2\omega_E+\omega_A)^{1/2} K_- - 2p\langle S^z\rangle e_S^+ \omega_A^{1/2} G_- \,|^2 \ . \tag{7}$$

The polarization dependence comes through the symmetric and antisymmetric combinations, $e_S^{\pm}$ and $e_A^{\pm}$, defined by

$$e_S^{\pm} = (e_1^z e_2^x + e_1^x e_2^z) \pm i(e_1^z e_2^y + e_1^y e_2^z) \ , \tag{8}$$

$$e_A^{\pm} = (e_1^z e_2^x - e_1^x e_2^z) \pm i(e_1^z e_2^y - e_1^y e_2^z) \ , \tag{9}$$

where $\mathbf{e}_1$ and $\mathbf{e}_2$ are unit polarization vectors for the incident and scattered light, respectively. Finally, the quantity $p$ in Eqs. (6) and (7) is a thermal factor; for $T \lesssim 0.5T_N$ it can be approximated by

$$p \simeq \langle S^z\rangle (2S-1)/2S^2 \ , \tag{10}$$

while its general form is quoted in Ref. 29. The coefficients $K_+$ and $G_+$ are, respectively, the linear and quadratic magneto-optic coupling coefficients for in-phase scattering, while $K_-$ and $G_-$ are the corresponding coefficients for out-of-phase scattering.

First, we analyze the data by considering only the in-phase contribution. This is because the deviation from tetragonal symmetry at a $Mn^{2+}$ site is relatively small, and so it is expected that the in-phase scattering will dominate. Some theory curves for $(XZ)$ polarization and different values of the ratio $G_+/K_+$ are shown in Fig. 9. These have been obtained using Eqs. (4) and (6), together with $e_S^- = -e_A^- = 1$ and the same exchange and anisotropy parameters as in Sec. III. The corresponding experimental data (the crosses in Fig. 3) show an increase with increasing temperature and the closest agreement is provided by theory curve $W$ indicating that $G_+/K_+$ is close to zero (i.e., $G_+/K_+ < 10^{-2}$). This contrasts with the behavior in $FeF_2$, where the quadratic magneto-optic coupling is important and recent estimates give $G_+/K_+ \simeq 0.44$ at the same excitation wavelength.[17]

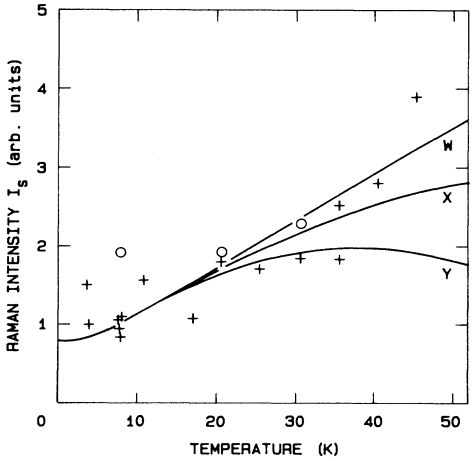


FIG. 9. Comparison of theory and experiment for the temperature dependence of the relative one-magnon integrated intensity (including the Bose population factor) in $MnF_2$. The theory curves correspond to zero out-of-phase scattering and the following values of $G_+/K_+$: $W$, 0; $X$, 0.01; $Y$, 0.1. See Fig. 6 for the experimental point notation.

The out-of-phase terms may also contribute to the scattered intensity and we illustrate their effect by some numerical examples in Fig. 10, taking the case of linear magneto-optic coupling ($G_+ = G_- = 0$) and $(XZ)$ polarization. Curves for in-phase scattering only ($K_- = 0$) and out-of-phase scattering only ($K_+ = 0$) are shown, together

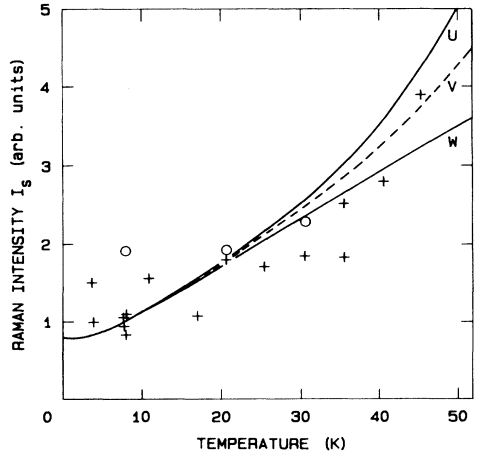


FIG. 10. As for Fig. 9, but this time taking the quadratic magneto-optic coefficients to be zero. The curves correspond to: $W$, $K_- = 0$; $U$, $K_+ = 0$; $V$, $|K_-/K_+| = 0.007$.

with an intermediate case. In fact, the predicted intensity $I_S$ is sensitive to even a relatively small amount of out-of-phase scattering, because the coefficient of $K_-$ in Eq. (7) is much larger than the coefficient of $K_+$ in Eq. (6) (since $\omega_E \gg \omega_A$ for $MnF_2$). The admixture of in-phase and out-of-phase scattering corresponding to the case $|K_-/K_+|=0.007$ in Fig. 10 is seen to give a good overall fit to the data across the temperature range. The effects of out-of-phase scattering in the presence of quadratic magneto-optic coupling can likewise be studied using Eqs. (4), (6), and (7).

The above analysis is sufficient to conclude that the dominant magneto-optic coefficient in $MnF_2$ is $K_+$, although small admixtures of other coefficients may occur. The differences in intensity, evident from Fig. 9, between $(XZ)$ polarization and $(YZ)$ polarization at the same temperatures are probably due to slight differences in the scattering volume (introduced by rotating the incident light polarization) or experimental uncertainties, and this polarization dependence cannot be used to obtain further information about the magneto-optic coefficients as we suggested previously.[11,12] On the other hand, comparison of Stokes intensities in $(XZ)$ and $(ZY)$ polarizations, or measurements of the anti-Stokes intensities in either polarization, would allow a more detailed analysis of the magneto-optic coefficients, by analogy with earlier work on $FeF_2$.[17]

The theory curves for the intensities in Figs. 9 and 10 have all been obtained assuming that $H_A(T) \propto \langle S^z \rangle^2$, since this case produced slightly better agreement with the magnon frequency versus $T$ data in Sec. III when magnon-magnon interactions were taken into account. However, very similar predictions for the intensity are found on taking $H_A(T) \propto \langle S^z \rangle$, and this can be understood as follows. We have seen that the $K_+$ magneto-optic coefficient is dominant for $MnF_2$; if only this term is retained, then it follows from Eqs. (3), (4), (6), and (7) that

$$I_S = A\langle S^z \rangle (n_M+1)\,|\,e_A^- K_+\,|^2 \omega_A/\omega_M \ . \tag{11}$$

At low temperatures the variation of $H_A(T)$ is unimportant; at higher $T$, such that $k_B T \gg \hbar\omega_M$ (e.g., $T \gtrsim 25$ K for $MnF_2$), we can approximate the Bose factor taking $(n_M+1) \sim k_B T/\hbar\omega_M$, and the right-hand side of Eq. (11) then has a temperature dependence given by $T\langle S^z \rangle/(2\omega_E+\omega_A)$. This last quantity depends only weakly on $\omega_A$ because $\omega_A \ll \omega_E$, and so the one-magnon *intensity* in a material where $K_+$ dominates is insensitive to the $T$ dependence of $H_A(T)$.

## V. ANALYSIS OF TWO-MAGNON SPECTRUM

### A. Theory

The two-magnon Raman scattering is strongly weighted by wave vectors near the Brillouin-zone boundary,[2,8] and it becomes important to include in the theory the effects of the smaller exchange terms $J_1$ and $J_3$. These were neglected compared with $H_A(T)$ and $J_2$ in discussing the one-magnon scattering from the $\mathbf{k} \approx \mathbf{0}$ excitations in Secs. III and IV. Symmetry considerations show that if $J_1$ and $J_3$ are taken to be zero the two-magnon scattering in $(YX)$ and $(YZ)$ [or $(XZ)$] polarizations should be identical, which is not the case experimentally (see Sec. II). The full expression for the magnon frequency $\omega(\mathbf{k})$ is[2]

$$\omega(\mathbf{k}) = \{\mu^2(\mathbf{k}) - [8\langle S^z \rangle J_2 \cos(\tfrac{1}{2}k_x a)\cos(\tfrac{1}{2}k_y a) \times \cos(\tfrac{1}{2}k_z c)]^2\}^{1/2} , \tag{12}$$

where

$$\mu(\mathbf{k}) = g\mu_B H_A(T) + 8\langle S^z \rangle J_2 - 4\langle S^z \rangle J_1 \sin^2(\tfrac{1}{2}k_z c) - 4\langle S^z \rangle J_3[\sin^2(\tfrac{1}{2}k_x a) + \sin^2(\tfrac{1}{2}k_y a)] . \tag{13}$$

It can be seen that at $\mathbf{k}=\mathbf{0}$ the terms in $J_1$ and $J_3$ disappear from the above expressions.

Although there have been several previous theoretical studies of two-magnon Raman scattering in $MnF_2$ (see Refs. 8 and 9 for review accounts), the more detailed experimental results of the present paper, which emphasize the polarization dependence of the scattering, necessitate further calculations. We make use of a finite-temperature perturbation method in the form recently applied to the rutile structure $FeF_2$.[10] In the case of $MnF_2$ it should be applicable for $T \lesssim 40$ K, and it is in this temperature range that the polarization differences are most pronounced. The formal theory for $MnF_2$ can be summarized as follows.

From symmetry arguments it can be deduced[2] that the Hamiltonian describing the interaction of light with the $MnF_2$ crystal has the approximate form

$$\tfrac{1}{2}\sum_{\mathbf{R},\boldsymbol{\delta}} \phi(\boldsymbol{\delta})(S^+_{\mathbf{R}} S^-_{\mathbf{R}+\boldsymbol{\delta}} + S^-_{\mathbf{R}} S^+_{\mathbf{R}+\boldsymbol{\delta}} + \gamma S^z_{\mathbf{R}} S^z_{\mathbf{R}+\boldsymbol{\delta}}) \tag{14}$$

for two-magnon scattering. Here $\mathbf{R}$ is summed over all magnetic sites, $\boldsymbol{\delta}$ is a vector connecting a magnetic site with one of its next-nearest neighbors on the opposite sublattice, and $\gamma$ is a weighting factor. Denoting $\sigma^\alpha(\boldsymbol{\delta}) = \mathrm{sgn}(\delta^\alpha)$ for $\alpha = x,y,z$, we have

$$\phi(\boldsymbol{\delta}) = B_1(e_1^x e_2^x + e_1^y e_2^y) + B_2 e_1^z e_2^z + B_3(e_1^x e_2^y + e_1^y e_2^x)\sigma^x(\boldsymbol{\delta})\sigma^y(\boldsymbol{\delta}) + B_4[e_1^y e_2^z + e_1^z e_2^y)\sigma^y(\boldsymbol{\delta})\sigma^z(\boldsymbol{\delta}) + (e_1^x e_2^z + e_1^z e_2^x)\sigma^x(\boldsymbol{\delta})\sigma^z(\boldsymbol{\delta})] + B_5[(e_1^y e_2^z - e_1^z e_2^y)\sigma^y(\boldsymbol{\delta})\sigma^z(\boldsymbol{\delta}) + (e_1^x e_2^z - e_1^z e_2^x)\sigma^x(\boldsymbol{\delta})\sigma^z(\boldsymbol{\delta})] . \tag{15}$$

This introduces the magneto-optic coefficients $B_1, B_2, \ldots, B_5$, while $\mathbf{e}_1$ and $\mathbf{e}_2$ are electric-field polarization vectors as defined before. By varying the experimental polarizations one can effectively pick out different $B$ coefficients or combinations of $B$ coefficients.

The intensity $I(\omega)$ for two-magnon scattering with frequency shift $\omega$ is found from a diagrammatic perturbation theory (including magnon-magnon interactions) to be pro-

portional to[10]

$$\frac{\langle S^z\rangle^2\mu(0)}{[1-\exp(-\hbar\omega/k_BT)]}\,\mathrm{Im}\left[\frac{G_0(\omega)}{1+tG_0(\omega)}\right], \tag{16}$$

where $\mu$ is defined in Eq. (13), and the quantities $G_0(\omega)$ and $t$ depend on the polarizations. For the rutile structure of $MnF_2$ there are three Raman-active modes, labeled $\Gamma_1^+$, $\Gamma_4^+$, and $\Gamma_5^+$ in a conventional notation.[30] In this work we have investigated experimentally the $\Gamma_1^+$ mode by means of $(XX)$ and $(ZZ)$ polarizations, the $\Gamma_4^+$ mode by $(YX)$ polarization, and the $\Gamma_5^+$ mode by $(YZ)$, $(ZX)$, and $(XZ)$ polarizations. The quantity $G_0(\omega)$ is

$$G_0(\omega)=\frac{1}{N}\sum_{\mathbf{k}}\frac{\mu(\mathbf{k})\Phi(\mathbf{k})\coth[\hbar\omega(\mathbf{k})/2k_BT]}{\omega(\mathbf{k})[\omega-2\omega(\mathbf{k})+2i\Gamma(\mathbf{k})][\omega+2\omega(\mathbf{k})+2i\Gamma(\mathbf{k})]}, \tag{17}$$

where $N$ is the number of magnetic sites in each sublattice, $\Gamma(\mathbf{k})$ is the one-magnon damping, and $\Phi(\mathbf{k})$ is a weighting factor for each mode[2]

$$\Phi(\mathbf{k})=\begin{cases}8\cos^2(\frac{1}{2}k_xa)\cos^2(\frac{1}{2}k_ya)\cos^2(\frac{1}{2}k_zc) \text{ for } \Gamma_1^+,\\ 8\sin^2(\frac{1}{2}k_xa)\sin^2(\frac{1}{2}k_ya)\cos^2(\frac{1}{2}k_zc) \text{ for } \Gamma_4^+,\\ 8\cos^2(\frac{1}{2}k_xa)\sin^2(\frac{1}{2}k_ya)\sin^2(\frac{1}{2}k_zc) \text{ for } \Gamma_5^+.\end{cases} \tag{18}$$

Finally the quantity $t$ in Eq. (16) is a magnon-magnon interaction parameter; on approximating for $|J_1| \ll J_2$ and $|J_3| \ll J_2$ as in $MnF_2$ it is given by[10]

$$t=\begin{cases}4J_2[H_A(T)+4\langle S^z\rangle J_2] \text{ for } \Gamma_1^+,\\ 4J_2[H_A(T)+8\langle S^z\rangle J_2] \text{ for } \Gamma_4^+ \text{ and } \Gamma_5^+.\end{cases} \tag{19}$$

The above expressions can be regarded as a generalization to finite temperatures of the theory of Elliott and Thorpe;[31] also Eq. (17) is derived employing a spin-wave ground state, instead of a Néel ground state as in Ref. 31.

Due to the weighting factors $\Phi(\mathbf{k})$, different critical points in the Brillouin zone are emphasized for the different Raman modes;[2] the $\Gamma$, $M$, and $R$ points are emphasized for the $\Gamma_1^+$, $\Gamma_4^+$, and $\Gamma_5^+$ modes, respectively. Hence the splitting in two-magnon peak frequencies between the $\Gamma_4^+$ and $\Gamma_5^+$ modes is expected to be of order

$$2[\omega(R)-\omega(M)]=8\langle S^z\rangle(J_3-J_1). \tag{20}$$

### B. Comparison with experiment

We now compare theory with experiment for temperatures up to about 40 K. Equations (12), (13), and (16)–(19) are employed, and we evaluate the summation over $\mathbf{k}$ in (17) in terms of a numerical integration over the Brillouin zone. The effective damping term $\Gamma(\mathbf{k})$ has, for simplicity, been replaced by an average zone-boundary damping $\Gamma_B$, since the two-magnon scattering is dominated by zone-boundary effects (except in the case of $\Gamma_1^+$ symmetry).[2] For comparison with the experiments of Sec. II the factor $\Gamma_B$ should also contain a contribution to represent the instrumental resolution. If the instrumental response is approximated by a Lorentzian then

$$\Gamma_B^{\mathrm{tot}}=\Gamma_B(T)+\tfrac{1}{2}\Gamma_R, \tag{21}$$

where $\Gamma_B(T)$ is the intrinsic one-magnon damping at the zone boundary and $\Gamma_R$ ($\simeq 0.9$ cm$^{-1}$) is the resolution half-width in the experiments. Approximate values for $\Gamma_B(T)$ may be deduced using a scaling argument[32] as in recent work on two-magnon scattering in $FeF_2$.[10]

In Figs. 11(a) and 11(b) the low-temperature (5.6 K) Raman spectra in $X(ZX)Y$ and $X(YX)Y$ polarizations are compared with theory. In each case the calculated line shape (dashed curve), obtained using parameters deduced

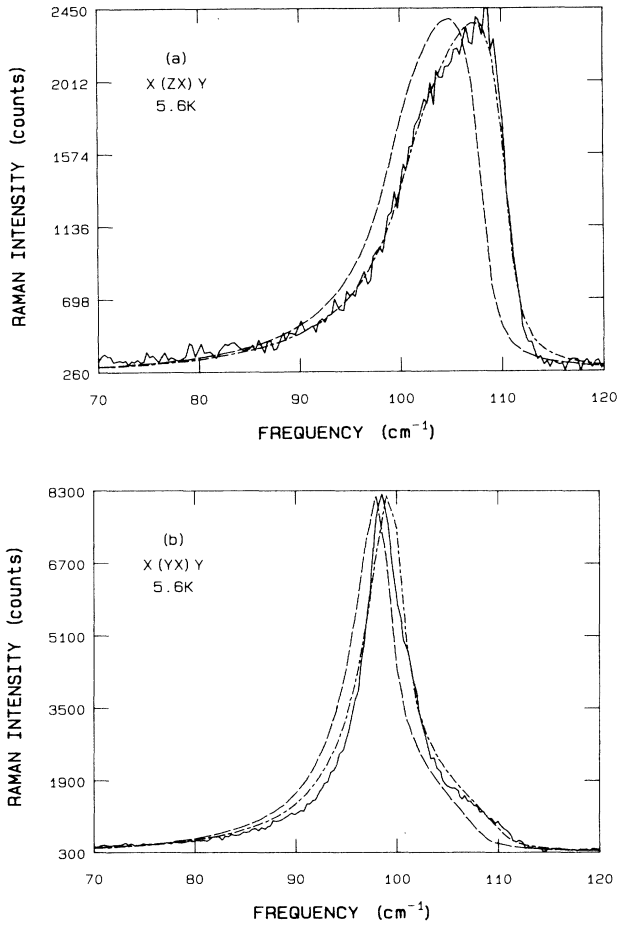


FIG. 11. Comparison of theory and experiment for the low-temperature two-magnon Raman spectrum of $MnF_2$ in (a) $X(ZX)Y$ and (b) $X(YX)Y$ polarizations. The theory curves given by the dashed and dot-dashed lines are discussed in the text. The integration time for the experimental points was 20 s.

from neutron scattering[19] (that is, $J_1=-0.44$ cm$^{-1}$, $J_2=2.45$ cm$^{-1}$, $J_3\approx 0$, and $g\mu_B H_A(0)=0.74$ cm$^{-1}$) and $\Gamma_B(0)\approx 0$, is very similar to the experimental spectrum but is shifted to a slightly lower frequency. An improved fit to the data is found by making a minor adjustment to the exchange constants (by amounts within their quoted uncertainties), and the theoretical spectra represented by dot-dashed curves in Fig. 11 were obtained assuming $J_1=-0.50$ cm$^{-1}$, $J_2=2.48$ cm$^{-1}$, $J_3\approx 0$, and $g\mu_B H_A(0)=0.74$ cm$^{-1}$. The calculated two-magnon spectrum for $\Gamma_1^+$ symmetry at $T<10$ K takes the form of a flat nonresonant band because of the weighting by the $\Gamma$ point in this case, and this is in accordance with the observed spectra in $(XX)$ and $(ZZ)$ polarizations. The use of a spin-wave ground state in the theory is an important factor in obtaining the excellent fits to the low-temperature spectra of Fig. 11.

The temperature dependences of the peak frequencies of the two-magnon scattering in off-diagonal polarizations, which correspond to $\Gamma_4^+$ and $\Gamma_5^+$ symmetries, are shown in Fig. 12. The frequency difference between the two modes is well accounted for by theory. The solid curves were calculated using the exchange parameters deduced from neutron scattering and the dashed curves correspond to the modified set of parameters mentioned above. Theory and experiment for the temperature dependence of the two-magnon linewidth and integrated intensity in $\Gamma_4^+$ and $\Gamma_5^+$ symmetries are compared in Figs. 13 and 14 and are found to be in agreement. For these cases the exchange parameters, as deduced from neutron scattering, were employed; essentially the same results are predicted with the other set of parameters. The spectral line shapes at higher temperatures $T\lesssim 0.6T_N$ are well reproduced by the theory provided the damping $\Gamma_B(T)$ is treated as an adjustable parameter. Thus until $\Gamma_B(T)$ for $MnF_2$ is known more precisely, detailed line-shape comparisons at higher temperatures, as performed for example for $KMnF_3$,[33] are not justified at present. The theoretical line shape of the two-magnon scattering in $MnF_2$ for temperatures $T>T_N$ has been investigated previously by Balucani *et al.*[34] and our experimental results are in good agreement with their calculations (compare our Fig. 3 and their Figs. 4–7).

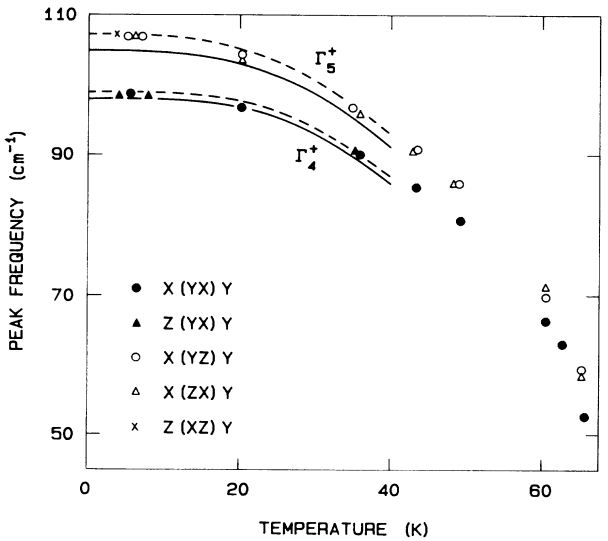


FIG. 12. Comparison of theory curves (see the text) and experimental points for the temperature dependence of the two-magnon peak frequency in $MnF_2$ for various polarizations.

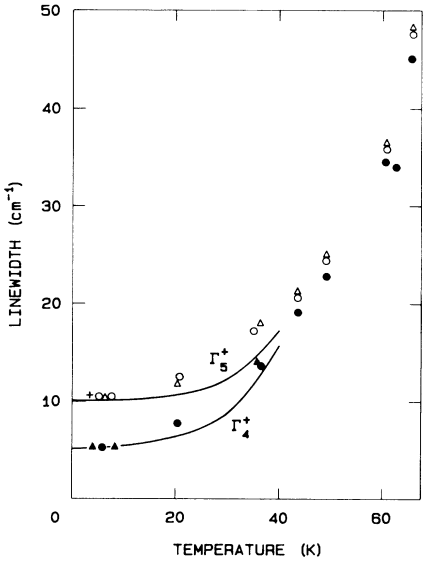


FIG. 13. Theory and experiment for the temperature dependence of the two-magnon linewidth (FWHM) in $MnF_2$ for various polarizations. The notation for the experimental points is given in Fig. 12.

By comparison between theory and experiment for the two-magnon intensities at low temperatures ($T\lesssim 10$ K) in various polarizations, we have been able to deduce (as in previous work[10] on $FeF_2$) the relative magnitudes of the magneto-optic coupling coefficients $B_i$ ($i=1,\ldots,5$) appearing in Eq. (15). The results for $MnF_2$ and $FeF_2$ are summarized in Table I, where the values are quoted relative to the largest coefficient $B_3$. It can be seen that the relative values of the coefficients in the two rutile-

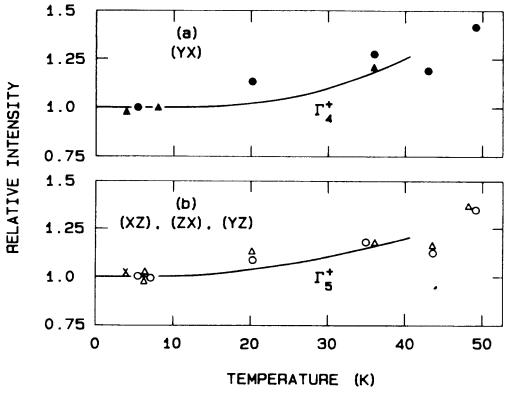


FIG. 14. Theory and experiment for the temperature dependence of the relative two-magnon integrated intensity (including the Bose population factor) for the (a) $\Gamma_4^+$ and (b) $\Gamma_5^+$ modes. The notation for the experimental points is given in Fig. 12.

TABLE I. Comparison of relative values of the magneto-optic coupling coefficients for two-magnon Raman scattering in the rutile-structure compounds $MnF_2$ and $FeF_2$.

| Compound | $\lvert B_1/B_3 \rvert$ | $\lvert B_2/B_3 \rvert$ | $\lvert B_4/B_3 \rvert$ | $\lvert B_5/B_3 \rvert$ | $\lvert B_6/B_3 \rvert$ | $\lvert B_7/B_3 \rvert$ |
|---|---|---|---|---|---|---|
| $MnF_2$ | 0.14 | 0.32 | 0.66 | 0.007 | | |
| $FeF_2$[a] | | 0.3 | 0.8 | $\sim 0$ | 0.05 | $\sim 0$ |

[a]Taken from Ref. 10.

structure compounds are remarkably similar. The coefficients $B_6$ and $B_7$ represent additional magneto-optic interactions that are allowed by symmetry but generally neglected;[10,31] they involve the spin operators in the combination $(S_R^+ S_{R+\delta}^- - S_R^- S_{R+\delta}^+)$ by contrast with Eq. (14). We were not able to deduce $B_6$ and $B_7$ for $MnF_2$ from the results of the present experiments.

We have also compared two-magnon integrated intensities $I(T)$ for temperatures $T \ll T_N$ (5 K) and $T \gg T_N$ (300 K), where the frequency moment theory of Brya and Richards[6] predicts $I(\infty)/I(0) \simeq 3.74$ for the combined Stokes and anti-Stokes scattering. The experimental spectra for $X(ZX)Y$, $X(YZ)Y$, $Z(XZ)Y$, and $Z(YZ)Y$ polarizations gave similar two-magnon intensities at each temperature, with an average ratio for $I(300\ \text{K})/(5\ \text{K})$ of $3.2 \pm 0.2$. Spectra in $X(YX)Y$ and $Z(YX)Y$ polarizations behaved likewise, but gave $I(300\ \text{K})/I(5\ \text{K}) = 3.9 \pm 0.5$. The integrated intensities were obtained from spectra recorded under similar conditions: They have not been corrected for absorption changes with temperature, as the absorption spectrum showed no noticeable dependence on polarization or on temperature (for temperatures between 77 and 300 K) at 476.5 nm. Although the difference between the two ratios lies just within the experimental uncertainty, it may be a real effect. On the other hand it may be due to the 300 K results in each polarization differing from the $T \to \infty$ limit of the theory. The present results are closer to the $I(\infty)/I(0)$ prediction of 3.74 than obtained in the earlier work of Brya and Richards,[6] who found $I(300\ \text{K})/I(2\ \text{K}) = 4.45$ for both $X(YX)Y$ and $X(YZ)Y$ polarizations with an excitation wavelength of 457.9 nm.

## VI. DISCUSSION AND CONCLUSIONS

We have reported the first observation of the weak one-magnon Raman scattering in pure $MnF_2$.[11,12] From a theoretical analysis of the integrated intensity as a function of temperature we showed that linear magneto-optic coupling (involving the coefficient $K_+$) provides the dominant effect, although small admixtures due to quadratic magneto-optic coupling and out-of-phase scattering may also be present. This contrasts with the one-magnon scattering from another rutile-structure antiferromagnet, $FeF_2$, which has also been studied in detail.[17] In $FeF_2$ the one-magnon scattering is much stronger and quadratic magneto-optic coupling plays an important role. The relative weakness of the one-magnon scattering in $MnF_2$ can be *partly* attributed to the small value of $\omega_A$, which appears in the numerator of Eq. (11), and *partly* due to differences in the magneto-optic coefficients for $MnF_2$ and $FeF_2$. For example, from Raman data on $MnF_2$ and $FeF_2$ (Ref. 17) recorded under similar conditions, we find for the ratio of one-magnon integrated intensities at approximately 10 K that

$$I_S(MnF_2)/I_S(FeF_2) \sim 10^{-2} . \tag{22}$$

*On the basis of linear magneto-optic coupling only* [using Eq. (11)] it can then be estimated that $K_+(MnF_2)/K_+(FeF_2) \approx 0.2$. However, if the quadratic magneto-optic coupling in $FeF_2$ is properly taken into account [using Eqs. (4), (6), and (7)], we find that $K_+(MnF_2)$ and $K_+(FeF_2)$ become more comparable in magnitude. We conclude that the quadratic coupling term has the effect of enhancing the intensity in $FeF_2$ relative to $MnF_2$. Because of the weak magneto-optic coupling and the low frequency of the magnon in $MnF_2$, it would be extremely difficult to observe any critical effect in the one-magnon scattering near $T_N$ using the Raman technique. However, such critical scattering may be observable with the Brillouin technique, as applied for example to $KNiF_3$.[35]

The two-magnon scattering in $MnF_2$ is considerably stronger than the one-magnon scattering. For example, the ratio of the integrated intensities of the two-magnon scattering in $Z(YX)Y$ polarization to the one-magnon scattering in $Z(XZ)Y$ polarization is $310 \pm 25$ at 8 K. From this ratio we can estimate the relative magnitudes of the linear and quadratic coupling coefficients $K_+$ and $B_3$, respectively. Using Eq. (4) for the one-magnon intensity and $T = 0$ expressions from Brya and Richards[6] for the two-magnon intensity, we deduce $K_+/B_3 \approx 0.5$ for excitation at 476.5 nm.

As can be seen from Table I, the *relative* $B$ coefficients for $MnF_2$ are quite similar to those of $FeF_2$, and the same is true for the *absolute* scattering intensities. The ratio of the integrated intensities of the $\Gamma_5^+$ two-magnon scattering in $MnF_2$ (476.5 nm excitation) and $FeF_2$ (514.5 nm excitation) is $0.82 \pm 0.05$. The corresponding ratio is $0.52 \pm 0.03$ with excitation at 647.1 nm for $FeF_2$. In deriving these ratios, corrections have been made for the frequency-to-the-fourth-power scattering law, but the spectrometer and photomultiplier responses have not been included. As the combined spectrometer and detector response is almost flat around 500 nm and then slowly falls with increasing wavelength, it is not possible to attribute the difference between the above ratios to mainly instrumental effects. There must also be a major contribution from the wavelength dependence of the scattering in $FeF_2$.

Comparisons can also be made with the ratio of coefficients $K_+/B_3$ for $FeF_2$. From earlier measurements[10,17] of the one- and two-magnon scattering in $FeF_2$ using excitation wavelengths of 514.5 and 647.1 nm, we estimate

$K_+/B_3 \approx 0.5$ in both cases. These estimates were obtained in the same manner as for $MnF_2$, but in addition allowing for the significant effect of the $G_+$ coefficient on the $FeF_2$ one-magnon intensity. The remarkable result is that the $K_+/B_3$ ratios are of the same order in $MnF_2$ and $FeF_2$.

In conclusion, this first detailed comparison of the magnitudes of the various coupling coefficients for two rutile structure compounds has revealed surprising similarities in many coefficients. The main difference between $MnF_2$ and $FeF_2$ lies in the significance of the quadratic magneto-optic coefficient $G_+$ in the one-magnon scattering in $FeF_2$. The quadratic coefficients are now seen to be of importance in determining the strength of the one-magnon scattering in certain insulators. The role of quadratic magneto-optic coupling has been demonstrated earlier for other iron compounds including $Y_3Fe_5O_{12}$,[36] $FeCl_2$,[37,38] and $FeBr_2$.[39] It would be informative to make similar detailed comparisons with antiferromagnets containing other metal ions to quantify further the relative significance of the linear and quadratic terms.

The present results for one- and two-magnon light scattering are seen to be in excellent agreement with theory for temperatures $T \lesssim 0.6T_N$. The theory for the one-magnon scattering including the effects of magnon-magnon interactions is expected to give closer agreement with experiment than the theory excluding such interactions,[9] and under this condition the theory taking $n=2$ gives best agreement with experiment for the temperature dependence of the magnon frequency. Thus we conclude that $n \simeq 2$ not only describes the temperature dependence of the anisotropy at low and high temperatures (see Sec III), but is most likely applicable for intermediate temperatures as well.

## ACKNOWLEDGMENTS

We are grateful to H. J. Labbé for the sample preparation. M.G.C. acknowledges support from the British Council, the National Research Council of Canada, and the United Kingdom Science and Engineering Research Council.

*Permanent address: Physics Department, University of Essex, Colchester CO4 3SQ, U.K.

[1]P. A. Fluery, S. P. S. Porto, and R. Loudon, Phys. Rev. Lett. **18**, 658 (1967).
[2]P. A. Fluery and R. Loudon, Phys. Rev. **166**, 514 (1968).
[3]P. A. Fluery, in *Light Scattering in Solids*, edited by M. Balkanski (Flammarion, Paris, 1971), p. 151.
[4]W. J. Brya, R. R. Bartkowski, and P. M. Richards, in *Magnetism and Magnetic Materials—1971 (Chicago)*, Proceedings of the 17th Annual Conference on Magnetism and Magnetic Materials, AIP Conf. Proc. No. 5, edited by C. D. Graham, Jr. and J. J. Rhyne (AIP, New York, 1972), p. 339.
[5]W. J. Brya, P. M. Richards, and R. R. Bartkowski, Phys. Rev. Lett. **28**, 826 (1972).
[6]W. J. Brya and P. M. Richards, Phys. Rev. B **9**, 2244 (1974).
[7]M. R. Poppinger, Z. Phys. B **27**, 69 (1977).
[8]U. Balucani and V. Tognetti, Riv. Nuovo Cimento **6**, 39 (1976).
[9]M. G. Cottam and D. J. Lockwood, *Light Scattering in Magnetic Solids* (Wiley, New York, 1986).
[10]M. G. Cottam, V. So, D. J. Lockwood, R. S. Katiyar, and H. J. Guggenheim, J. Phys. C **16**, 1741 (1983).
[11]M. G. Cottam and D. J. Lockwood, Phys. Rev. B **31**, 641 (1985).
[12]M. G. Cottam and D. J. Lockwood, J. Magn. Magn. Mater. **54-57**, 1143 (1986).
[13]D. J. Lockwood, in *Light Scattering in Solids III*, edited by M. Cardona and G. Güntherodt (Springer-Verlag, Heidelberg, 1982), p. 59.
[14]J. P. Gosso and P. Moch, Physica B **89**, 209 (1977).
[15]E. Montarroyos, S. S. Vianna, Cid B. de Araujo, S. M. Rezende, and A. R. King, J. Magn. Magn. Mater. **31-34**, 557 (1983).
[16]A. K. Ramdas, J. Appl. Phys. **53**, 7649 (1982).
[17]D. J. Lockwood, M. G. Cottam, V. C. Y. So, and R. S. Katiyar, J. Phys. C **17**, 6009 (1984).
[18]F. M. Johnson and A. H. Nethercot, Phys. Rev. **114**, 705 (1959).
[19]A. Okazaki, K. C. Turberfield, and R. W. H. Stevenson, Phys. Lett. **8**, 9 (1964); O. Nikotin, P. A. Lindgård, and O. W. Dietrich, J. Phys. C. **2**, 1168 (1969).
[20]F. Keffer, Phys. Rev. **87**, 608 (1952).
[21]F. Keffer, in *Handbuch der Physik*, edited by H. P. J. Wijn (Springer-Verlag, Heidelberg, 1966), Vol. 18/2, p. 1.
[22]T. Oguchi, Phys. Rev. **111**, 1063 (1958); see also J. Kanamori and M. Tachiki, J. Phys. Soc. Jpn. **17**, 1384 (1962).
[23]J. C. Burgiel and M. W. P. Strandberg, J. Phys. Chem. Solids **26**, 877 (1965).
[24]M. G. Cottam and R. B. Stinchcombe, J. Phys. C. **3**, 2326 (1970).
[25]R. B. Stinchcombe and T. L. Reinecke, Phys. Rev. B **9**, 3786 (1974).
[26]See, for example, the detailed account by A. B. Harris, D. Kumar, B. I. Halperin, and P. C. Hohenberg, Phys. Rev. B **3**, 961 (1971), and references therein.
[27]J. Solyom, Zh. Eksp. Teor. Fiz. **55**, 2355 (1968) [Sov. Phys.—JETP **28**, 1251 (1969)].
[28]M. P. Schulhof, R. Nathans, P. Heller, and A. Linz, Phys. Rev. B **4**, 2254 (1971).
[29]M. G. Cottam, J. Phys. C. **8**, 1933 (1975).
[30]J. O. Dimmock and R. G. Wheeler, Phys. Rev. **127**, 391 (1962).
[31]R. J. Elliott and M. F. Thorpe, J. Phys. C **2**, 1630 (1969); see also M. F. Thorpe, J. Appl. Phys. **41**, 892 (1970).
[32]C. R. Natoli and J. Ranninger, J. Phys. C **6**, 345 (1973).
[33]D. J. Lockwood and G. J. Coombs, J. Phys. C **8**, 4062 (1975).
[34]U. Balucani, V. Tognetti, and M. G. Pini, Il Nuovo Cimento B **46**, 81 (1978).
[35]K. B. Lyons and P. A. Fleury, Phys. Rev. Lett. **48**, 202 (1982).
[36]W. Wettling, M. G. Cottam, and J. R. Sandercock, J. Phys. C **8**, 211 (1975).
[37]G. Mischler, D. Bertrand, D. J. Lockwood, M. G. Cottam, and S. Legrand, J. Phys. C **14**, 945 (1981).
[38]G. C. Psaltakis and M. G. Cottam, J. Phys. C **15**, 4847 (1982).
[39]G. C. Psaltakis, G. Mischler, D. J. Lockwood, M. G. Cottam, A. Zwick, and S. Legrand, J. Phys. C **17**, 1735 (1984).